

Creep Behavior of a New Cast Austenitic Alloy

John P. Shingledecker, Philip J. Maziasz*, Neal D. Evans*, and Michael J. Pollard***

*Oak Ridge National Laboratory, Oak Ridge, TN, USA

** Caterpillar Technical Center, Peoria, IL, USA

Abstract:

A new cast austenitic alloy, CF8C-Plus, has been developed by Oak Ridge National Laboratory (ORNL) and Caterpillar for a wide range of high temperature applications including diesel exhaust components and turbine casings. The creep strength of CF8C-Plus is over ten times greater than that of the standard cast CF8C stainless steel and comparable to the highest strength wrought commercial austenitic stainless steels and alloys, such as NF709. The creep properties of CF8C-Plus will be discussed in terms of alloy design methodology and the evaluation of long-term creep tested specimens (over 20,000 hours). Microcharacterization shows that the excellent creep strength is due to the precipitation of very fine nano-scale and stable MC carbides without the formation of deleterious intermetallic phases.

Keywords: creep, austenitic alloys, stainless steels, castings, engineered microstructure, MC carbides

1.0 Introduction

Advanced heavy truck diesel engines must continue to have higher fuel efficiency as well as reduced exhaust emissions, without sacrificing durability and reliability. More demanding normal duty cycles require exhaust manifolds and turbocharger housing materials to withstand temperatures ranging from 70 to above 750°C. Such materials must withstand both prolonged, steady high-temperature exposure as well as more rapid and severe thermal cycling. New emissions reduction technology and transient power excursions can push temperatures in these critical components even higher. The current material of choice for many of these exhaust component applications is SiMo cast iron, but it is being pushed beyond its high-temperature strength and corrosion limitations. Another application opportunity comes from turbine manufacturers seeking lower-cost alternatives to nickel-based superalloy castings for casings and large structural components, as temperatures are pushed beyond the limits of current cast ferritic materials. These needs lead to a cooperative research and development agreement (CRADA) between the Caterpillar (CAT) Technical Center and Oak Ridge National Laboratory (ORNL) to investigate various cast stainless steel materials for advanced diesel engine components. One development of this work was a new cast austenitic stainless steel, CF8C-Plus, which showed dramatic improvements over SiMo cast iron and standard CF8C steel in creep, thermal fatigue, high-temperature tensile strength, and aging response (impact toughness). In this paper, the excellent creep properties of CF8C-Plus are discussed in terms of micro-characterization data for this alloy during aging and testing. The 'engineered microstructure' approach used to develop the alloy is emphasized, and some of the other potential industrial applications are noted.

2.0 Alloy Design Methodology

The 'engineered microstructure' methodology that is being used at ORNL to develop new alloys, specifically austenitic stainless steels and nickel-based superalloys, is the product of over 20 years of experience on nuclear reactor cladding materials, originally part of the U.S. DOE Fusion Reactor Materials research programs [1]. Work on creep-resistant wrought stainless steels was continued on the U.S. DOE Fossil Energy Advanced Materials research programs, which produced a variety of new alloys including the High-Temperature Ultrafine-Precipitation-Strengthened (HT-UPS) steels, which are the only austenitic stainless steels having a creep strength comparable to Ni-based superalloys [2]. Now, with the development of CF8C-Plus steel, this alloy design methodology has been successfully applied to austenitic stainless steel castings for the DOE Energy Efficiency and Renewable Energy programs.

The general concept for developing an austenitic stainless steel with good high temperature strength is to produce a target service microstructure consisting of a high-strength matrix phase with a fine (nano-scale, if possible) dispersion of stable precipitates (resistant to coarsening). This microstructural design concept also includes eliminating deleterious aging-induced phases (sigma, Laves, etc.) and controlling the precipitation along grain boundaries. The four alloying rules or effects that must be understood and applied are: Reactant Effects, Catalytic Effects, Inhibitor Effects, and Interference Effects [3]. Reactant effects are simply how certain elements directly react to form phases; for example: Nb and C forming NbC. Catalytic effects describe how elements that are not reactants affect the rate of phase formation involving other elements; for example: silicon dramatically enhances Fe₂Mo laves phase formation. Inhibitor effects are somewhat the opposite of catalytic effects in that certain elements can retard the kinetics or increase barriers to the formation of other phases; for example: carbon and boron can retard or eliminate the formation of sigma or Laves phase. Finally, interference effects are simply a way of understanding how elements compete with one another in complex alloy systems; for example Ti can form both TiC and TiN. These four rules include obvious concepts based on both thermodynamic driving forces and kinetic phenomenon, and are primarily based on experimental studies using modern nano-scale microstructural and microcompositional analysis using analytical electron microscopy (AEM) techniques. Currently, thermodynamic prediction software, such as ThermoCalc, has not been as useful for the design austenitic alloys compared to its widespread use in Ni-based and ferritic alloy design because appropriate detailed databases are not available. Recent neural network models have been applied successfully to predicting phase formation in some common austenitic systems [4], but there is still much work left to be done before such tools can predict the microstructural evolution in complex alloy systems. Although it is not strictly a computational tool, the engineered microstructure approach is currently the most useful framework for the design of complex austenitic stainless steel alloys.

3.0 Design of CF8C-Plus

The nominal chemical compositions (wt%) for casting alloys: CF8C, CF8C-Plus, SiMo cast iron, and Ni-resist austenitic cast iron; and wrought alloys: 347HFG, Super 304H, NF709, and Alloy 617 are shown in Table 1. CF8C is the casting grade of type 347 stainless steel. It is nominally a 19Cr-10Ni stainless steel that is solid-solution strengthened prior to service, but it is capable of significant carbide precipitation hardening during high-temperature service. Niobium carbides (NbC) and chrome carbides (M₂₃C₆) provide the precipitation strengthening.

Table 1. Nominal Alloy Compositions (wt%)

| | Cr | Ni | Fe | Mn | Mo | Nb | C | Si | Other |
|----------------|------|------|------|-----|-----|------|------|-----|----------------------|
| <i>Cast</i> | | | | | | | | | |
| CF8C | 19.0 | 10.0 | Bal. | <1 | 0.3 | 0.80 | 0.07 | 1.0 | |
| CF8C-Plus | 19.0 | 12.5 | Bal. | 4.0 | 0.3 | 0.80 | 0.10 | 0.5 | 0.25N |
| SiMo | | | Bal. | 0.3 | 0.6 | | 3.45 | 4.0 | |
| Ni-Resist | 2.0 | 35.0 | Bal. | 0.5 | | | 1.90 | 5.0 | |
| <i>Wrought</i> | | | | | | | | | |
| TP347HFG | 18.0 | 10.0 | Bal. | 1.6 | | 0.80 | 0.08 | 0.6 | |
| Super 304H | 18.0 | 9.0 | Bal. | 0.8 | | 0.40 | 0.10 | 0.2 | 3.0Cu, 0.1N |
| NF709 | 20.0 | 25.0 | Bal. | 1.0 | 1.5 | 0.20 | 0.15 | 0.5 | 0.1Ti |
| Alloy 617 | 22.0 | Bal. | 1.5 | 1.0 | 9.0 | | 0.10 | 1.0 | 1.2Al, 12.5Co, 0.4Ti |

In stabilized or overstabilized austenitic stainless steel castings, such as CF8C, delta ferrite is present in the as-cast microstructure. These materials typically show excellent aqueous corrosion resistance, particularly to sensitization. However, delta-ferrite can rapidly transform to sigma (σ) phase during prolonged high-temperature exposure. Because sigma phase is embrittling, the first design requirement for CF8C-Plus was to produce a stabilized 100% austenite microstructure, free of delta ferrite. Typical austenite stabilizers include Ni, Mn, C, and N, all of which were added in precise amounts based upon the alloying rules. In addition to being an austenite stabilizer, Mn has the added benefit of increasing the solubility of N in austenite. When the Ni and Cr equivalents for CF8C are plotted on a Schaeffler diagram in figure 1, we see that the alloy is predicted to have between 10 and 15% delta ferrite present. Comparatively, the CF8C-Plus should be austenite without residual delta ferrite. The Schaeffler diagram does not take into account the added stability N brings to austenite. A digital Fisher ® Feritscope ® was used to measure the ferrite number for both the CF8C and CF8C-Plus steel castings. The CF8C had a ferrite number of 16.8 +/-1.1, which is equivalent to 14% delta ferrite, and the CF8C-Plus did not register any detectable ferromagnetic behavior, meaning it has less than 0.1% delta ferrite. Both of these macroscopic measurements are in excellent agreement with the predictions from the Schaeffler diagram.

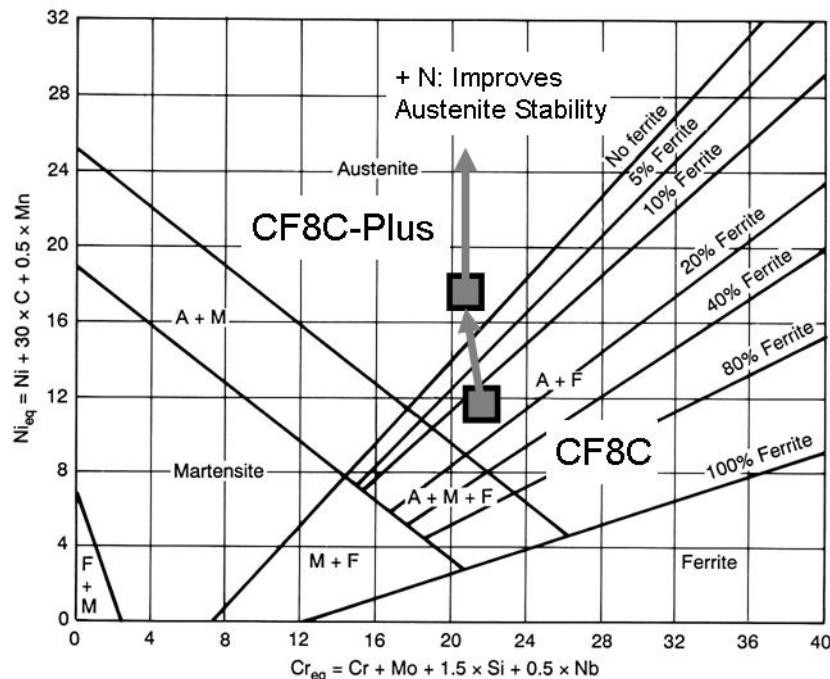


Figure 1. Schaeffler Diagram [5] showing Ni and Cr equivalents for CF8C and CF8C-Plus

A second design requirement for the CF8C-Plus was to increase the strength of the austenite matrix. The addition of N is known to increase the strength of an austenite matrix and Mn is also well known to increase the strain-hardening rate; thus it was anticipated that the individual N and Mn effects as well as their synergistic effects would improve tensile, creep, and fatigue strength. Because Nb, Cr, and C were present in both the CF8C and CF8C-Plus, NbC and $M_{23}C_6$ would provide the primary precipitation strengthening, and it was not known if there would be large differences between the precipitate size, location, and morphology. As discussed later, the CF8C-Plus showed nano-scale MC carbide precipitation which appears to mainly be an effect of the Mn addition and results in a dramatic improvement in creep strength compared to CF8C.

The third design requirement was having strong and ductile interdendritic regions. It was anticipated that replacing the delta-ferrite with carbides might initially reduce the ductility in these interdendritic regions in the as-cast material, but after prolonged aging the dendritic regions of the CF8C-Plus were expected to show better ductility due to the absence of sigma phase. Furthermore, the Si content was also reduced to mitigate the formation of Laves phase. Thus, the design philosophy was to eliminate all of the detrimental phases in the dendritic regions, leaving only carbides for strengthening.

Figure 2 shows the as-cast microstructures (etched) for CF8C (left) and CF8C-Plus (right). As anticipated, the CF8C shows large FeCr delta-ferrite in the interdendritic regions, while the CF8C-Plus shows a combination of carbides and the absence of delta-ferrite. Micron-size NbC are observed in the CF8C and CF8C-Plus. The typical microstructure for SiMo cast iron is shown in figure 3. Large graphite nodules are observed throughout the matrix.

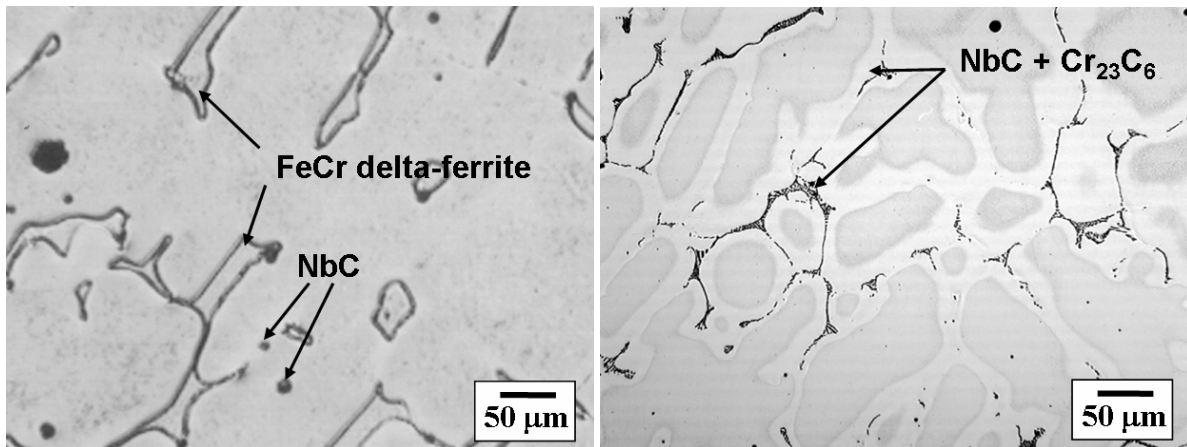


Figure 2. Microstructure of polished and etched as-cast CF8C (left) and CF8C-Plus (right)

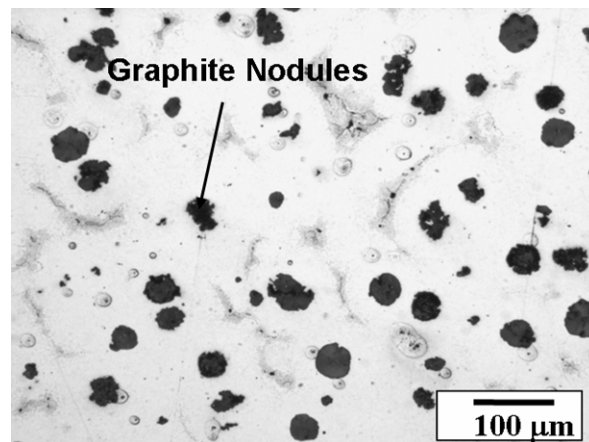


Figure 3. Microstructure of polished and etched as-cast SiMo cast iron

4.0 Alloy Development and Testing

The initial development of CF8C-Plus was done using 2 laboratory scale heats (15lbs). A number of elevated temperature tensile tests, simple thermo-mechanical fatigue tests, and a few exploratory creep tests showed a significant improvement in all areas of mechanical behavior. At this point, the decision was made to produce several modified 500lb commercial heats of the best material. Thus, after less than two years of lab-scale development and testing, commercial material was produced. Later, more commercial heats of material were made using both typical static sand castings and centrifugal casting technology and reproducible data was obtained. The CF8C-Plus alloy exhibited excellent fluidity due to

the addition of Mn, and thin-wall casting were easily produced. Further research to explore cooling rate effects was performed on lab scale heats cast in graphite blocks. Thus, the creep data presented in this paper cover 2 laboratory scale heats and 2 commercial heats of CF8C-Plus and two heats of CF8C. Commercially produced SiMo cast iron and a high Ni austenitic casting, Ni-Resist (Ni-rich austenitic cast iron), were also obtained for comparison testing because engine exhaust components are made with these alloys. Creep testing was performed between 650°C and 850°C at constant load for initial stresses ranging from 35 to 200 MPa.

5.0 Creep Behavior

Figure 4 shows typical creep strain versus time curves for CF8C and CF8C-Plus steels. These curves were obtained by creep testing identical commercially produced centrifugal castings of CF8C and CF8C-Plus and a lab-scale graphite block casting of CF8C-Plus. The test condition is 750°C and 140MPa. The CF8C-Plus steel shows over an order of magnitude (10 times) improvement in creep-rupture life over an identical casting of CF8C. The plot also suggests that there is a cooling rate effect on the creep properties of CF8C-Plus steel. For the static graphite block casting (fast cool), the rupture life was extended roughly 6 times (less than 1 order of magnitude) over the slower cooled centrifugal casting. Additionally, the CF8C-Plus steel shows a four-fold improvement in ductility over CF8C steel (7% for CF8C and 27% to 35% for CF8C-Plus). The general improvement in rupture ductility is clearly observed in figure 5, which is a plot of rupture elongation versus time for all of the various creep-rupture tests on CF8C and CF8C-Plus stainless steels. The CF8C has poorer ductility most probably due to the formation of the sigma phase (which can embrittle grain boundaries as well as reduce oxidation resistance at the boundaries because it is Cr-rich), whereas CF8C-Plus was designed to eliminate such formation of sigma phase.

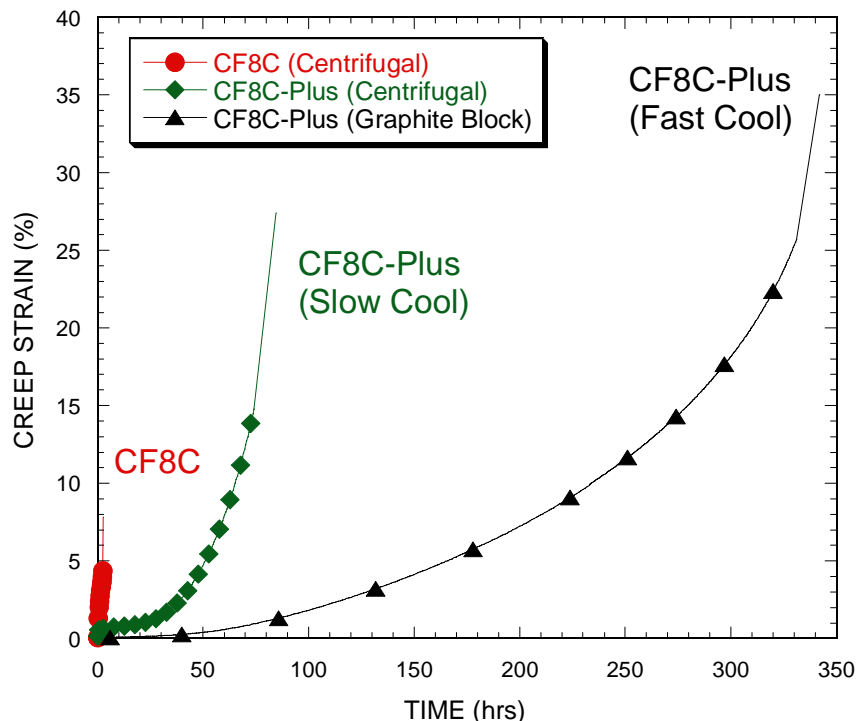


Figure 4. Creep Strain vs Time Curves for CF8C and CF8C-Plus Centrifugal Castings (Slow Cooling Rate) and CF8C-Plus cast in graphite (fast cooling rate) tested at 750°C and 140MPa

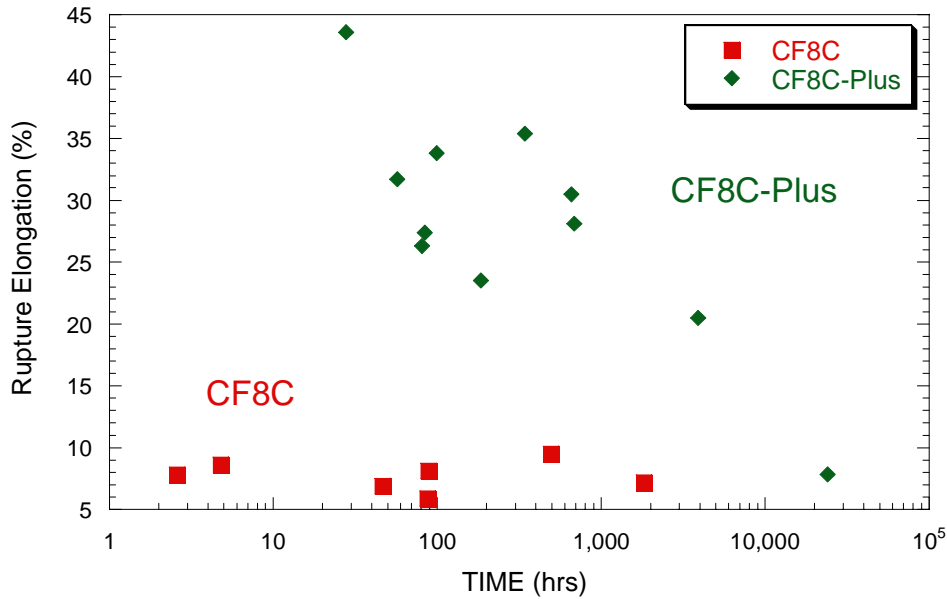


Figure 5. Rupture Elongation vs. Time for CF8C and CF8C-Plus tested between 650 and 850°C at 35 to 200 MPa. CF8C-Plus does not form embrittling grain boundary phases resulting in excellent rupture ductility compared to CF8C

To evaluate the creep behavior of CF8C-Plus over a range of times, temperatures, and stresses, the rupture strength of CF8C-Plus is plotted using the Larson-Miller Parameter (LMP) with the rupture strength of commercial CF8C, Ni-Resist, SiMo castings given in figure 6. A LMP constant of 20 was arbitrarily chosen as is typical for general materials comparisons and does not represent an optimized fit of the CF8C-Plus data. As previously described, the data on CF8C covers a wide range of temperatures, stresses, and times from a large variety of castings. All CF8C-Plus castings show a significant improvement in creep strength compared to the other diesel exhaust component alloys. For other applications, including large turbine casings, particular importance should be given to the difference between the creep strength of CF8C and CF8C-Plus steels. For a given stress level between 35 and 200MPa, the average LMP value for CF8C-Plus is approximately 1500 higher than CF8C. This is equivalent to a 35X improvement in rupture life at 700°C or a 60°C improvement in temperature for equivalent rupture life at 100,000 hour.

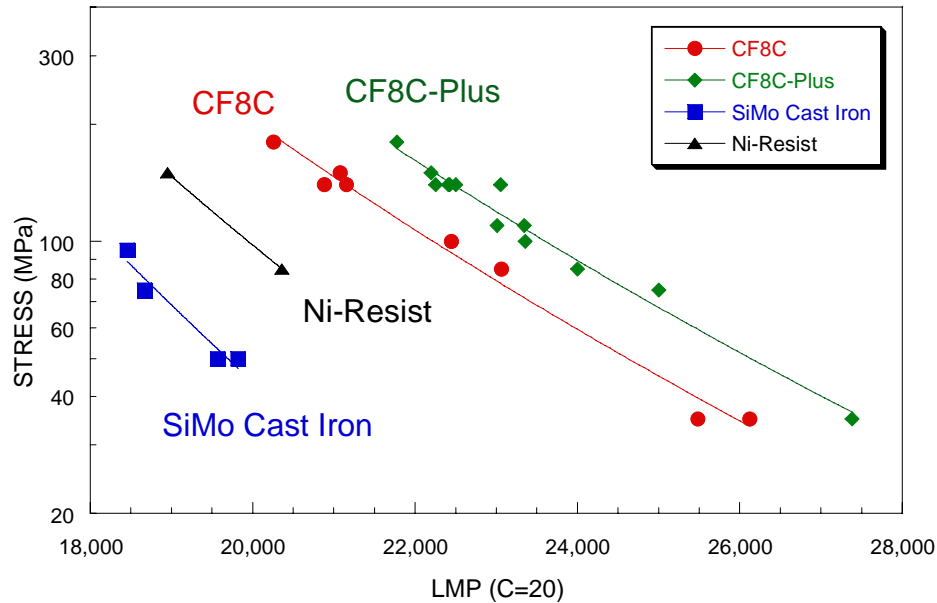


Figure 6. Larson-Miller Parameter plot showing candidate diesel exhaust alloys. CF8C-Plus shows superior creep strength compared to current alloys

The origins of the improvements in creep strength of CF8C-Plus compared to CF8C were summarized in the previous alloy design approach section. Nitrogen was specifically added to improve the strength of the austenite matrix as well as the austenite stability, and Mn was added to increase the solubility of N and improve the strain-hardening behavior. However, the unexpected result of these additions was the large differences observed in the nucleation of the MC (NbC) carbide precipitate structures. Figure 7 shows transmission electron microscopy (TEM) images of CF8C and CF8C-Plus after creep testing at 850°C and 35MPa. The CF8C (left-hand side image) ruptured after 493 hours, while the CF8C-Plus (right-hand side image) ruptured after 24,100 hours. In the CF8C, larger NbC, on the order of 200 to 300 nm, are widely dispersed throughout the matrix. By contrast after over 20,000 hours, fine NbC, much less than 50 nm in diameter, are closely spaced and uniformly dispersed throughout the matrix. These fine MC carbides nucleate on the dislocation structure and form very early during creep; this provides Orowan pinning of dislocations by incoherent precipitates which reduces the amount of strain accumulated during primary creep and prolongs the secondary creep regime. The dislocations, seen bowing between MC carbide pinning sites in the CF8C (indicative of climb) are clean, without fine precipitates.

For the CF8C-Plus stainless steel, this kind of microstructure has been characterized in some wrought austenitic alloy systems, including a group of HT-UPS steels [6]. These high-temperature ultra-fine precipitate (HT-UPS) stainless steels had a creep strength on the order of nickel-based superalloys such as alloy 617 due to the formation of fine MC carbides [2]. To achieve the dense dispersion of nano-scale carbides and high creep strength, a dislocation structure was needed on which the MC carbides, that have a much larger volumetric misfit relative to the matrix, could preferentially form. This also necessitates the absorption of vacancies, which then paralyzes the dislocations and prevents climb-glide. High density dislocation network concentrations were produced in the HT-UPS steels by warm or cold working the material prior to testing. If the HT-UPS steel was not deformed prior to testing, the nano-scale MC particles would not have the dislocations as nucleation sites and only large MC particles would form, thus reducing the creep strength.

The results of the current research on stainless steels are intriguing because both of the materials investigated are castings, so deformation processes are not involved in creating a dislocation structure

upon cooling. One possible explanation for the differences in structure is that the addition of Mn alters the stacking fault energy (SFE) of the CF8C-Plus, giving rise to higher energy stacking faults. Extrinsic stacking faults bounded by partial dislocations, which grow by emitting vacancies, have long been known to be the preferred nucleation sites for highly oversized misfit precipitations such as NbC [7]. The precipitation of NbC at these dislocations aids the growth of the stacking fault by a multi-stage process involving the climb of the partial dislocation and the emission of vacancies. This process is iterative resulting in stacking faults decorated with NbC, often in the form of loops. A change in the stacking fault energy of the system would be a factor in the size and spacing of such precipitates and more dissociated dislocations would be expected in the CF8C-Plus stainless steel. Another factor that could effect NbC nucleation could involve the presence of Mn and N in the CF8C-Plus steel. There is analytical electron microscopy (AEM) data on nano-scale NbC precipitates in stainless steels that indicate they have a relatively pure phase composition which does not incorporate many of the other alloying elements [8]. If the fine NbC particles must reject Mn into the matrix in order to grow, that would suggest slower growth kinetics in the CF8C-Plus steel compared to CF8C. It would follow that, since nucleation and growth are competing processes during early stage precipitation, the CF8C-Plus would favor more nucleation, if the driving forces for precipitation are similar in both steels. Furthermore, if the NbC are truly carbides and not 'carbo-nitrides' that many envision (no NbN have been observed in these steels and similar alloys), then the growth of NbC must also reject N at the interface. This would also favor more nucleation of NbC, which would pin the dislocations better, further enhancing continued fine NbC precipitation at those heterogeneous nucleation sites. The right-side image in figure 7 is consistent with strings of fine NbC particles having nucleated along the same dislocation segments. A third possibility for the differences between the two steels is the presence of ferrite in the CF8C and not the CF8C-Plus steel. In this case, residual stresses, due to thermal expansion/contraction upon cooling, should be lower in the ferrite containing CF8C steel. However, cracks have not been detected in any of the CF8C-Plus steel castings produced to date, and the tensile data shows an increase in ductility over CF8C; therefore, these stresses are probably small. The apparent improvements in creep strength due to fast cooling may be due to the trapping of more dislocation or vacancies which would enhance the rate of nucleation the NbC. Obviously, more detailed electron microscopy analysis on the material pre- and post-test is needed to fully understand the observed phenomenon.

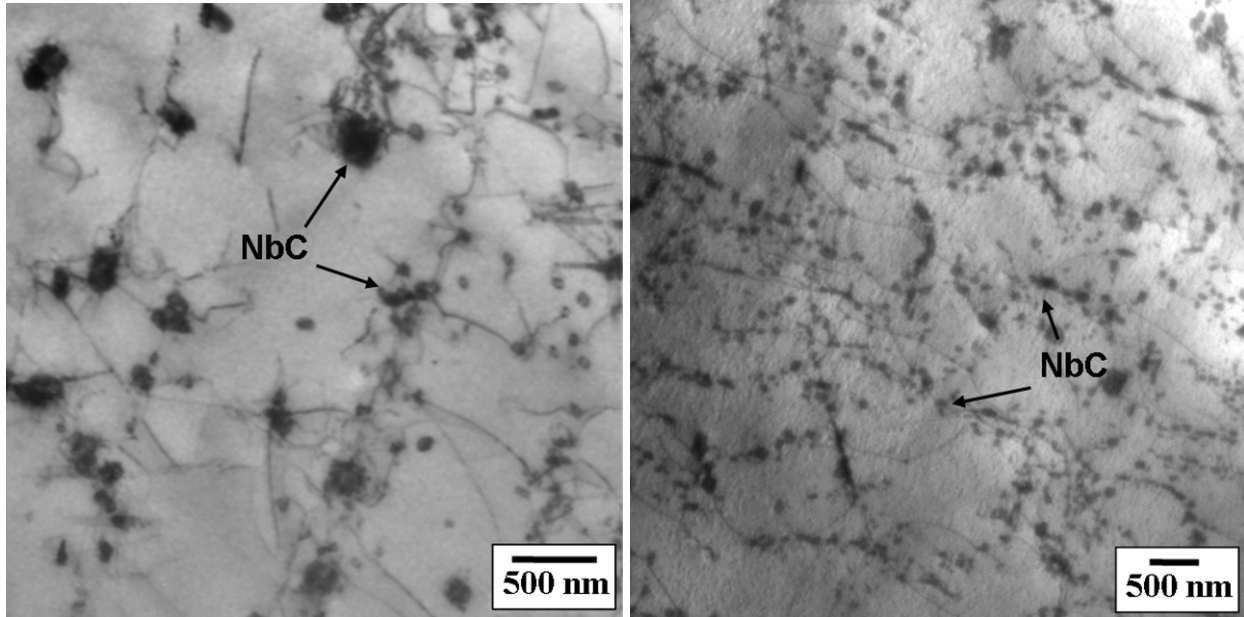


Figure 7. TEM image of CF8C (left) and CF8C-Plus (right) after creep testing at 850°C and 35MPa for 493 hours (CF8C) and 24,100 hours (CF8C-Plus). The CF8C-Plus shows a uniform distribution of nano-sized NbC after 23,000 hours while the CF8C shows coarse NbC.

6.0 Applications for CF8C-Plus

One of the primary drivers in choosing a material for diesel engine exhaust components is cost. The cost of SiMo cast iron is much lower than the other cast alloys shown in figure 6 and listed in Table 1. The cost of CF8C-Plus, however, should be similar to CF8C due to the small increases in Ni, Mn, and N. Ni-Resist, having over 30% Ni, can cost the same or slightly more than other austenitic stainless steel castings. The significant strength difference between the CF8C-Plus and the SiMo would allow for much thinner-section components, which would reduce weight and cost of a finished component. The enhanced corrosion resistance of CF8C-Plus over SiMo cast iron also allows for thinner parts. However, direct replacement of SiMo with CF8C-Plus probably also requires component redesign due to the large differences in the physical properties of the materials, and to take advantage of the much higher creep strength of the CF8C-Plus. Currently, Ni-resist is also used in certain exhaust manifold applications, but its creep resistance is not much better than SiMo cast iron. CF8C-Plus stainless steel can directly replace Ni-resist for exhaust manifolds where creep deformation or distortion might be a concern without the need to extensively redesign the part [9]. For diesel engine applications, CF8C-Plus offers a cost-effective solution and direct performance upgrade relative to Ni-Resist austenitic cast iron without the need to try more expensive Ni-based superalloy castings. Additionally, CF8C-Plus is a significant high-temperature upgrade for current SiMo components which cannot last long at target temperatures, but part redesign is necessary to make such an upgrade cost effective.

In addition to diesel exhaust applications, CF8C-Plus has potential for a variety of other high-temperature applications, including large castings for gas and steam turbine casing components. Some smaller industrial gas turbines already utilize CF8C stainless steel for its corrosion resistance, and in this case, replacing the components with CF8C-Plus would increase reliability and allow for increased temperatures/pressures to be used. There is precedence for austenitic stainless steel casings being used in steam turbines. Eddystone Unit #1 has a steam turbine with an inner cylinder made of a type 316 stainless steel casting and has various other 316 wrought components including the nozzle block [10]. This unit, built in 1961, has been operating for over 40 years in the ultrasupercritical steam regime. The original conditions in this steam turbine, 648°C main steam temperature, were higher than the most 'advanced'

steam turbines in the world today, but these steam conditions were later downgraded to ensure reliable operation [11]. In only the past 5 years have new ultrasupercritical steam power plants been built with steam temperatures higher than the Eddystone unit. CF8C-Plus steel is a superior casting alloy to type 316 (cast equivalent CF8Mo or HF grades) and most other stainless steels in terms of creep strength, tensile strength, and ductility. For comparison, the CF8C-Plus rupture strength is plotted in figure 8 using the LMP against some of the stronger wrought stainless steels (see Table 1 for compositions). The Ni-based alloy 617 is included for comparison. CF8C-Plus shows creep strength similar to NF709, and it appears to retain its strength at much lower stresses/longer times compared to the Nb, N, and Cu strengthened Super 304H. Current research on the next generation of ultrasupercritical steam turbines in Europe under the AD700 program has identified cast alloys 625 and 617 as candidates for high-temperature casings. In this case, the premise is that the current 9-12 Cr ferritic steels used as casings will not have the strength or corrosion resistance needed for steam temperatures near 700°C [12]. CF8C-Plus has the potential for steam turbine casings as an alternate to Ni-based alloy casings. In this case, the creep-rupture strength may not be as high as candidate nickel-based alloys, but CF8C-Plus would have a tremendous cost advantage. Thus, U.S. research on USC turbine materials is currently evaluating the potential of austenitic alloys in steam turbines [13].

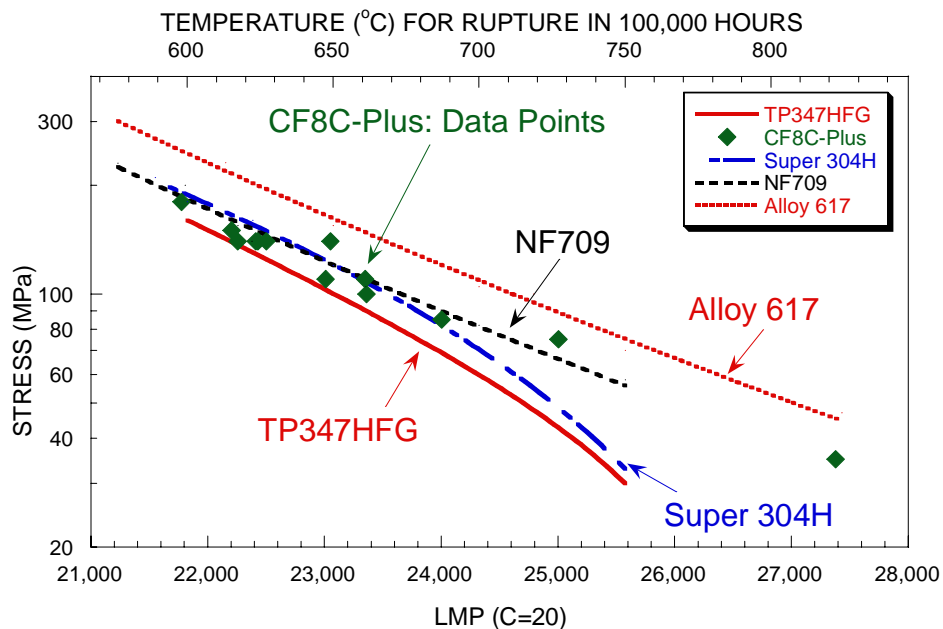


Figure 8. Larson-Miller Parameter plot showing CF8C-Plus compared to high-strength wrought austenitic alloys and the Ni-based alloy 617. The top abscissa gives the estimated temperature (°C) for rupture in 100,000 hours. The creep strength of CF8C-Plus is as good or better compared to the best commercial wrought stainless steels.

An additional factor in the cost of producing a casting is the post-casting stress relief or solution heat-treatment typically required for stainless steel castings. Standard practice for CF8C is to solution treat after casting at 1050°C. CF8C-Plus steel does not require a post-casting heat-treatment, which results in a substantial reduction in time and money for the casting producer. This cost savings can be very high for large components, such as steam turbine casings, where large furnaces have to be erected in the field. In terms of castability, CF8C-Plus exhibits excellent melt fluidity due to the increase levels of Mn. Even with its reduction in Si, still added to enhance of melt fluidity (Si is not widely used a deoxidizer today), the castability of CF8C-Plus steel is as good or better than CF8C steel. For these reasons, thin-walled components and thick-section components can both be readily produced out of CF8C-Plus steel.

7.0 Conclusions

The cast austenitic stainless steel CF8C-Plus was developed using the engineered microstructure approach for alloy design. Creep testing on both laboratory and commercial heats of CF8C-Plus steel shows over an order of magnitude increase in creep-rupture life accompanied by an increase in rupture ductility compared to standard CF8C. This strength advantage is consistent over a wide range of temperatures and stresses. More over, these strength advantages are found in the as-cast condition and require no additional post-casting heat-treatment. Electron microscopy of long-term creep tested specimens show this strength is due, in part, to a very stable distribution of fine nano-scale NbC precipitates. More research is currently underway to better understand the fundamental mechanisms associated with this stable structure. When compared to current diesel exhaust alloys, CF8C-Plus steel has a significant creep strength advantage and can be used cost effectively as a replacement for SiMo cast iron and Ni-Resist austenitic iron. Further evaluation of the alloy shows that its strength is comparable to the best commercial wrought stainless steels including NF709 and comes close to that of the Ni-based superalloy 617. This makes it an attractive candidate alloy for large turbine component applications including steam and gas turbine casings.

Acknowledgements

This research was sponsored by CRADAs in the Heavy Vehicle Propulsion Materials Program within the Office of FreedomCAR and Vehicle Technologies in the DOE under the Assistant Secretary for Energy Efficiency and Renewable Energy (EERE), and includes financial support from Caterpillar, Inc. It was also sponsored in part by an appointment to the ORNL Postmaster's Research Participation Program administered by the Oak Ridge Institute for Science and Education (ORISE) and ORNL, and was supported (ORNL SHaRE User Center) by the Division of Materials Sciences and Engineering, Office of Basic Energy Sciences, U.S. Department of Energy.

References

1. P.J. Maziasz. "Microstructural Stability and Control for Improved Irradiation Resistance and for High-Temperature Strength of Austenitic Stainless Steels." *Special Technical Publication 979*, ASTM, PA, 1988: 116-161.
2. P.J. Maziasz. "Developing an Austenitic Stainless Steel for Improved Performance in Advanced Fossil Power Facilities." *Journal of Metals*. Vol. 41, No. 7, July 1989: 14-20.
3. P. Maziasz and M. Pollard. "High-Temperature Cast Stainless Steel." *Advanced Materials & Processes*, October 2003, Vol. 161, No. 10: 57-59
4. T. Sourmail, H.K.D.H. Bhadeshia, and D.J.C. MacKay, "Neural network model of creep strength of austenitic stainless steels." *Materials Science and Technology*, June 2002, Vol. 18: 655-663
5. D.J. Kotecki, "Welding of Stainless Steels." ASM Handbook, Volume 6, Welding, Brazing, and Soldering, ASM International, December, 1993: 678-707
6. R.W. Swindeman, P.J. Maziasz. "The Mechanical and Microstructural Stability of Austenitic Stainless Steels Strengthened by MC-Forming Elements." *Creep: Characterization, Damage, and Life Assessments, Proceedings of the Fifth International Conference on Creep of Materials*. ASM International, OH, 1992. 33-42.
7. J.M. Silcock and W.J. Tunstall. "Partial Dislocations Associated with NbC Precipitation in Austenitic Stainless Steels." *Philosophical Magazine*, Vol. 10, 1964. 361-389.
8. P.J. Maziasz, "Molybdenum Solubility Differences in MC Phases Formed in Titanium and Niobium Modified Austenitic Stainless Steels Using AEM." *Proceedings of the 42nd Annual Meeting of the Electron Microscopy Society of America*. © 1984, San Francisco Press, Inc. 496-497
9. Personal communication between P.J. Maziasz and industrial contacts
10. J.H. Harlow. "Metallurgical Experience with the Eddystone 5000 lb/in² 1200°F Unit No. 1." *Joint International Conference on Creep. Institute of Mechanical Engineers*, London U.K., 1963. 7-11 to 7-20.

11. J.F. Henry, J.D. Fishburn, I.J. Perrin, E.S. Sadlon, C.T. Ward. "Advanced Supercritical Technology: Back to the Future." *Proceedings to the Fourth International Conference on Advances in Materials Technology for Fossil Power Plants (Hilton Head, SC, Oct. 25-28, 2004)*. ASM-International, Materials Park, OH, 2005.
12. R. Blum, R.W. Vanstone. "Materials Development for Boilers and Steam Turbines Operating at 700°C." *Parsons 2003 - Proceedings of the Sixth International Charles Parsons Turbine Conference, Institute of Materials, Minerals, and Mining, London, 2003*. 489-510.
13. P.J. Maziasz, I.G. Wright, J.P. Shingledecker, T.B. Gibbons, and R.R. Romanowsky. "Defining of the Materials Issues and Research for Ultrasupercritical Steam Turbines." *Proceedings to the Fourth International Conference on Advances in Materials Technology for Fossil Power Plants (Hilton Head, SC, Oct. 25-28, 2004)*. ASM-International, Materials Park, OH, 2005.